Wire electrical discharge machining at high relative speeds

Author(s):
Weingärtner, Eduardo; Wegener, Konrad; Kuster, Friedrich

Publication date:
2012

Permanent link:
https://doi.org/10.3929/ethz-a-007569011

Wire electrical discharge machining at high relative speeds

Eduardo Weingärtner[a,*], Konrad Wegener[a] , Friedrich Kuster[a]

[a]Institute of Machine Tools and Manufacturing (IWF), ETH Zurich, Tannenstrasse 3, 8092 Zurich, Switzerland

Phone: +41 44 632 0495

Fax: +41 44 632 11 25

weingaertner@iwf.mavt.ethz.ch

Abstract

In order evaluate the influence of high relative speeds on wire electrical discharge machining (WEDM), single discharge experiments were carried out inside a grinding machine, in a self-designed wire electrical discharge dressing device (WEDD-Device). The shape and size of the eroded craters, measured on the workpiece/anode, were found to be highly influenced by the relative speed. Based on the shape of eroded craters, the expansion speed of the crater radius can be calculated and the slip of the plasma's center point during the discharge can be measured. Additionally, the volume of the eroded craters was found to increase as relative speed increases, indicating that higher melting efficiencies are achieved for higher relative speeds. Finally, an electro-thermal model is described and simulation results are discussed, which helps to better understand the influence of the relative speed on the erosion process.

Keywords: Wire EDM; Single discharge; Relative speed; Electro-thermal model.

1. Introduction

In wire electrical discharge machining (WEDM), the wire electrode is fed from a spool at feed speeds typically ranging from 2 to 20 m/min. Since the workpiece normally stays stationary during erosion, this feed speed represents the final relative speed between wire and workpiece. If short discharge durations are taken as reference, as normally in WEDM, the resulting relative speed during a single discharge can be neglected. Assuming a wire feed speed of 20 m/min and discharge duration of 1.5 µs, the wire moves only 0.5 µm throughout the entire discharge duration, which is very little compared to the size of eroded craters, which, depending on the discharge energy, can be hundreds of times larger than that. However, in some applications, the workpiece rotates during the erosion process. Cylindrical wire electrical discharge turning (CWEDT) is an example of such a process. According to Haddad and Tehrani (2008) and Mohammadi et al. (2008), in CWEDT a rotary axis is added to the machine to manufacture axisymmetric parts. Wire electrical discharge grinding (WEDG), first proposed by Masuzawa et al. (1985), is similar to CWEDT in its concept, but uses a wire guide for further guiding the wire at the erosion zone. Still, in both

cases relatively low rotation speeds have been applied. According to Weingärtner et al. (2010b), in wire electrical discharge dressing (WEDD), a process that is primarily designed for on-machine and in-process dressing, higher rotational speeds are used, in some cases even more than 100 m/s, since the grinding wheel has to be dressed at grinding speeds. Now, assuming a speed of 100 m/s and discharge duration of 1.5 μs, a relative displacement of 150 μm between wire and workpiece occurs during the entire discharge.

In this paper, the influence of high relative speeds on WEDM is assessed. Single discharge experiments were carried out for relative speeds up to v_r=80 m/s. In order to assist in the interpretation of experimental results, an electro-thermal model was proposed. Simulation and experimental results are then compared and discussed in the following sections.

2. Experimental setup

The erosion tests were carried out on an especially designed WEDD-unit (wire electrical discharge dressing unit), which was integrated into a universal cylindrical grinding machine Studer type S31. This WEDD-unit was originally designed and manufactured by Weingärtner et al. (2010b) for dressing metal bonded grinding wheels and is mounted on the support of the internal grinding spindle. This WEDD-device is composed basically of a two axes feed system and a wire drive system. The axes are controlled by an adaptive control system ‘‘AC Progress VP4’’ – GF AgieCharmilles, which allows high dynamic erosion gap regulation. Furthermore, a special wire guide, proposed by Weingärtner et al. (2010a), is applied to the erosion zone to minimize wire vibrations and its influence on the erosion material removal rate and quality of the grinding wheel surface.

As tool electrode, a zinc-coated brass wire from Bedra was applied (CobraCut type S with a diameter of 0.33 mm). The workpiece electrode was a brass wheel of diameter 75 mm, with the following specification: CuZn39Pb3. This brass wheel was previously ground with a fine grained grinding wheel, to allow for a good surface quality and facilitate the subsequent measurement of eroded craters. Standard grinding oil from Blaser Swisslube (Blasogrind HC5) was used as dielectric for all erosion tests. **Fig. 1** shows a schematic representation of the single discharge experimental setup. The workpiece rotates at a specific relative speed v_r and the wire travels along the workpiece axial direction, tangential to the circumferential surface of the workpiece. The erosion pause interval time t_o was set to be as long as possible, so that consecutive discharges can be measured separately. The shape and volume of the eroded craters were measured using an optical 3D measurement device Alicona InfiniteFocus.

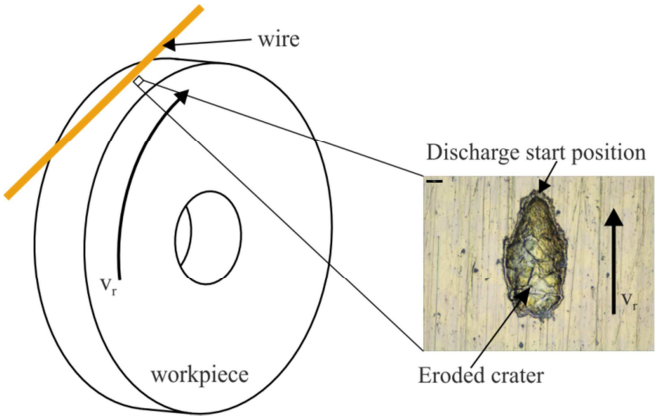

Fig. 1. Schematic representation of experimental setup for performing WEDM single discharge tests.

The discharge duration time of different pulses were measured using an oscilloscope type LeCroy WaveRunner 44MXi-A. The discharge time cannot be directly specified on the control system ‘‘AC Progress VP4”. The machine operates using capacitors for delivering the electrical current, so that the discharge time depends on the stored electrical energy and how fast it can be delivered after the breakdown phase. For peak currents of I_{peak}=58 and 73 A, the measured discharge times correspond to t_e=1.15 and 1.20 µs respectively.

3. Influence of the relative speed on WEDM single discharges

According to Uhlmann et al. (2005), a relative speed between workpiece and tool electrode influences the EDM process in such a way that small crater areas are generated by increasing speeds above 2,5 m/s (measurements up to 5 m/s were carried out on electrical discharge turning process). Haddad and Tehrani (2008) and Wang et al. (2006) point out that the relative speed affects the efficiency of the erosion process to a great extent, where the erosion material removal rate decreases by increasing relative speed. On the other hand, Matoorian et al. (2008) describe just the opposite, stating that the material removal rate can be increased by increasing the relative speed. According to Kunieda and Kameyama (2010) the discharge plasma slides easier over the cathode rather than over the anode. They carried out die-sinking erosion experiments using relatively long discharge pulses (discharge duration of about 200 µs).

In this work, single discharge experiments were carried out using typical WEDM parameters, where short discharge durations and high peak currents were applied. The shapes of eroded craters are first presented on **Fig. 2**. Different relative speeds up to v_r=80 m/s were applied for two different peak current values. It can be seen, that the relative speed has a significant influence on the shape of the eroded craters. The plasma channel slides over the workpiece/anode during the discharge, creating an elongated crater along the relative speed direction. **Table 1** summarizes the erosion parameters applied during these experiments.

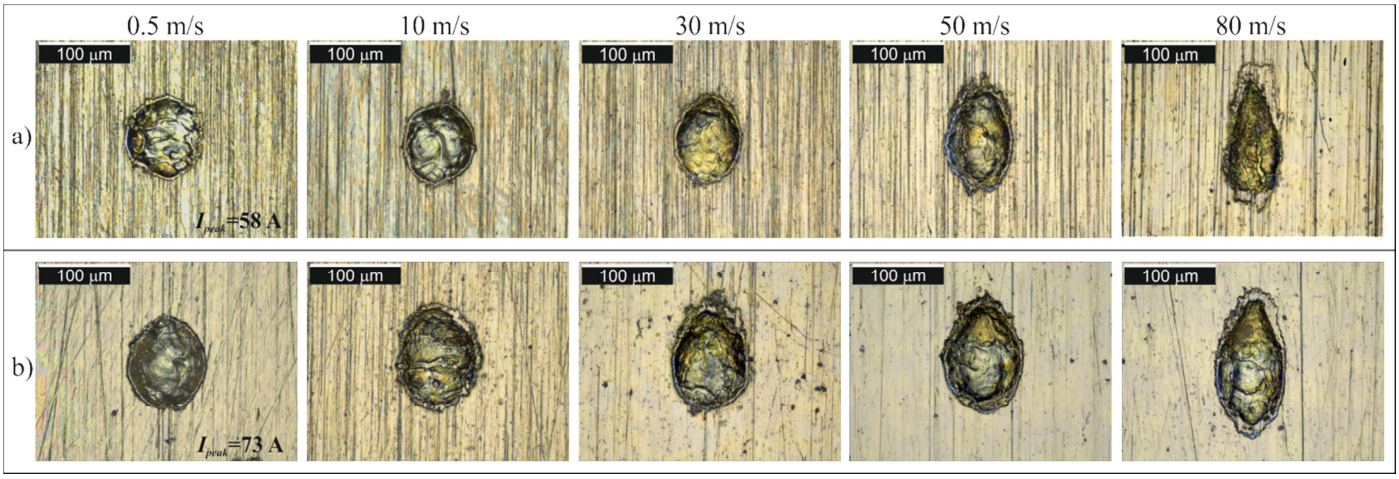

Fig. 2 – Influence of relative speed on the shape of eroded craters: a) I_{peak} = 58 A, t_e = 1.15 µs; b) I_{peak} = 73 A, t_e = 1.20 µs.

Table 1. Set of parameters used on single discharge experiments.

discharge duration	t_e	1,15 µs (Fig. 2a); 1.20 µs (Fig. 2b)
peak current	I_{peak}	58 A (Fig. 2a); 73 A (Fig. 2b)
pause interval time	t_o	400 µs
relative speed	v_r	0,5-80 m/s
oil flow rate	Q_l	25 L/min
wire diameter	d_w	0.33 mm
wire type		CobraCut S
Workpiece		Brass (CuZn39Pb3)
Workpiece polarity		Anode

To show quantitatively how the shape of eroded craters change due to the relative speed between workpiece and wire electrode, the minor and major diameters of different craters were measured. **Fig. 3** shows the results obtained by applying a peak-current of I_{peak}=58 A and relative speeds starting from v_r=0.5 m/s up to 80 m/s.

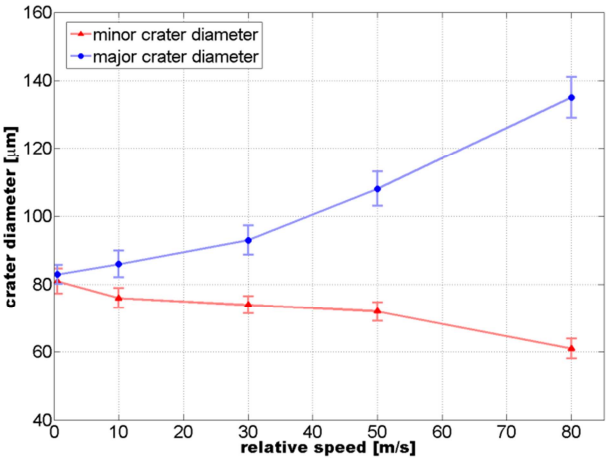

Fig. 3. Crater diameters for different relative speeds (I_{peak} = 58 A, t_e = 1.15 µs).

The crater extends along the relative speed direction (major diameter) and decreases slightly perpendicular to it (minor diameter). In this example, the major diameter is more than twice as big as the minor diameter when a relative speed of v_r=80 m/s is applied. Based on the shape of craters shown in **Fig. 2** and the measurements presented in **Fig. 3**, it can be observed that, at least for this type of WEDM discharges, the plasma easily slides over the anode.

Moreover, the elongated shape of the craters can reveal how the plasma slides over the workpiece/anode during a single discharge. The theoretical slip is calculated based on the discharge duration t_e and applied relative speed v_r. **Fig. 4** illustrates two different craters, eroded by using different peak currents and the same relative speed of v_r=80 m/s.

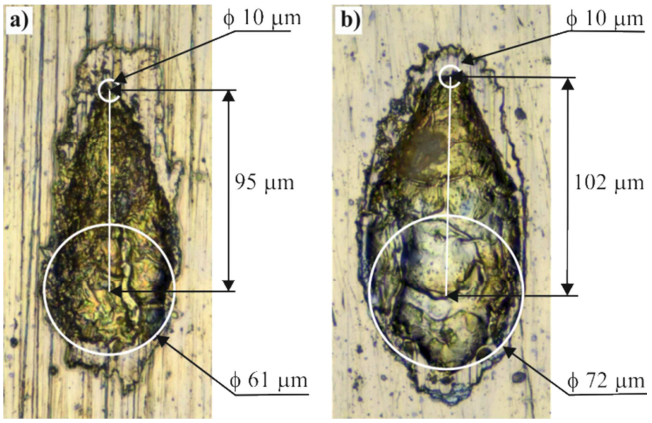

Fig. 4 – Slip of plasma arc during single discharges. a): I_{peak}=58 A, t_e=1.15 µs; b) I_{peak}=73 A, t_e=1.20 µs.

In **Fig. 4a**, theoretically, the center point of the plasma should slide 92 µm during one single discharge ($80\ \mu m/\mu s \cdot 1.15\ \mu s\ = 92\ \mu m$). The white circles, one small and another larger, indicate, respectively, the start and end position of the of the center point of the plasma. The distance measured between centers is 95 µm. In **Fig. 4b**, the crater was eroded by applying a peak current of I_{peak}=73 A. The center point of the plasma should slide, theoretically, 96 µm ($80\ \mu m/\mu s \cdot 1.20\ \mu s\ = 96\ \mu m$), and the measured distance between the center points of both white circles equals 102 µm. In both cases, theoretical and measured slips are very well correlated.

3.1 Expansion speed of crater radius

Since we know that the theoretical slip of the plasma matches the measured slip, another interesting aspect can be observed, namely the expansion speed of the crater radius. **Fig. 5** illustrates important quantities that should be used to quantify it. One can observe that the crater radius increases linearly in the beginning and reaches a maximum after a certain time. More precisely, the crater reaches a diameter of 72 µm (white circle) after a slip of 70 µm. In this case, the crater radius grows up to 36 µm within 0.87 µs (70 µm/80 µm/µs), corresponding to an expansion speed of approximately 41 m/s (36 µm/0.87 µs).

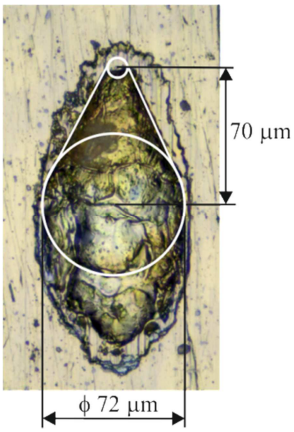

Fig. 5 – Method for quantifying the expansion speed of the crater radius.

For a peak current of I_{peak}=73 A and discharge duration of t_e=1.20 µs, the crater radius stops increasing after reaching a diameter of 72 µm. At this moment during the discharge, the current density has already started to decrease, since the peak current was reached in the middle of the discharge time (capacitor discharge). This information is important helps describing the heat source that is used in the WEDM erosion model described later in this paper.

3.2 Influence of the relative speed on the eroded crater volume

The eroded craters were further evaluated and their eroded volumes were measured using an optical 3D measurement device *Alicona InfiniteFocus*. The results obtained by applying a peak current of I_{peak}=73 A are presented in **Fig. 6**. The relative speed between the electrodes has proved to influence not only on the shape of the crater, as shown in **Fig. 2**, but also on the amount of eroded volume per crater. As shown in **Fig. 6**, the eroded volume per crater varies between approximately $1x10^{-4}$ µm^3 and $2x10^{-4}$ µm^3 by as the relative speed is increased from v_r=0.5 m/s to 80 m/s.

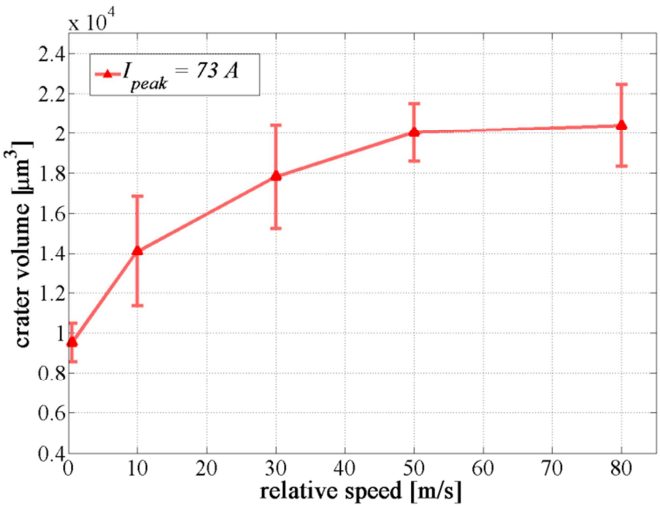

Fig. 6 – Influence of relative speed on eroded volume of single craters (I_{peak}=73 A, t_e=1.20 µs).

One possible explanation to the curve behavior in **Fig. 6** is related to the melting efficiency of the process. According to Van Elsen et al. (2007), melting efficiency can be defined as "the ratio of the minimal amount of energy needed to warm up and melt a given amount of material to the added energy". For a stationary heat source, where no relative speed is applied, the discharge energy is also used for overheating the melting pool, leading to a worse melting efficiency. On the other hand, when a relative speed is applied, the discharge energy is better used to warm up melt more material. The way how the discharge energy influences the eroded volume as relative speed is increased needs to be further investigated. For different discharge pulses, a maximum on the eroded volume curve is expected to be located at different relative speeds. Less energetic pulses must have a maximum located at lower speeds while more energetic pulses must have a maximum shifted to higher relative speeds.

4. WEDM model

To better understand the effect of the relative speed on the eroded craters, an electro-thermal model was developed to describe WEDM single discharges. First, the model approach is described, followed by a discussion about simulations results, which are then compared with experimental results.

4.1 WEDM single discharge model approach

The WEDM model is based on the heat conduction phenomenon, assuming that the heat generated in the plasma is transmitted to the workpiece via a time dependent heat source, which grows from a point to a disc and moves relative to the surface of the workpiece during the discharge duration. According to Incropera et al. (2006), the partial differential equation that describes the heat conduction in cartesian coordinates is can be expressed as

$$\frac{\partial^2 T}{\partial x^2}+\frac{\partial^2 T}{\partial y^2}+\frac{\partial^2 T}{\partial z^2}+\frac{\dot{q}}{k}=\frac{1}{\alpha}\cdot\frac{\partial T}{\partial t} \tag{1}$$

where T is the temperature, x, y and z represent the cartesian coordinate system, $\dot{q}$ is the rate of energy generation per unit volume (W/m^3), k is the thermal conductivity ($W/m\cdot K$), α the thermal diffusivity (m^2/s) and t represents the time.

This equation can be solved numerically by finite-difference techniques, where time and space are discretized and the temperature is solved for different discrete nodal points. In this model approach, three different types of nodal points were considered: adiabatic nodes (nodal points on the workpiece surface, excluding those in contact with the heat source), interior nodes and nodes in contact with the heat source. The finite-difference equations used for solving the temperature in different nodal points are presented in **Table 2**. These equations describe a tree-dimensional system, where the distance between consecutive nodal points was chosen to be equal ($\Delta x=\Delta y=\Delta z=0.5$ μm). The interval time Δt separates successive temperature

calculations and has to obey a stability criterion described in **Table 2**. Since a small value of Δx is used and due to small values of material diffusivities α, very short time intervals Δt have to be used.

Table 2. Mathematical description of the thermo-physical erosion model (Transient, three dimensional finite-difference equations). Δt is the time interval, Δx the distance between two consecutive nodal points, ρ represents the mass density (kg/m^3), c_p is the specific heat at constant pressure (J/kg·K) and q'' represents the heat flux (W/m^2).

Interior nodes	$T_{m,n,p}^{t+1} = Fo\left(T_{m-1,n,p}^{t} + T_{m+1,n,p}^{t} + T_{m,n-1,p}^{t} + T_{m,n+1,p}^{t} + T_{m,n,p-1}^{t} + T_{m,n,p+1}^{t}\right) + (1-6Fo)T_{m,n,p}^{t}$
Adiabatic nodes	$T_{m,n,p}^{t+1} = Fo(2T_{m-1,n,p} + T_{m,n+1,p} + T_{m,n-1,p} + T_{m,n,p+1} + T_{m,n,p-1}) + (1-6Fo)\cdot T_{m,n,p}^{t}$
Heat source	$T_{m,n,p}^{t+1} = Fo(2T_{m-1,n,p} + T_{m,n+1,p} + T_{m,n-1,p} + T_{m.n,p+1} + T_{m,n,p-1}) + \frac{2Fo\cdot q''\cdot\Delta x}{k} + (1-6Fo)\cdot T_{m,n,p}^{t}$
Fourier number	$Fo = \frac{\alpha\cdot\Delta t}{(\Delta x)^2}$; Stability Criterion $Fo \le \frac{1}{6}$

The heat source (heat flux q'') used as input for the model is defined as

$$q'' = \frac{I\cdot U}{\pi\cdot r_c^2} \quad (2)$$

where I is the current, U is the burning voltage and r_c is the crater radius.

The burning voltage U was assumed to be constant at 20 V for all simulations. The current as function of time was measured for different discharge pulses and used as input for the simulations. The dimension of the crater radius r_c is based on the shape of eroded craters shown in **Fig. 2**, which depended on the discharge time and peak current. The heat source was discretized assuming different values for each time step. The pulse duration time was measured for different peak currents, and used as input for the model. Temperature-dependent material properties are taken into consideration, especially the heat capacity c_p and thermal conductivity k of the workpiece material. A new Fourier number Fo, which represents the ratio of the heat conduction rate to the rate of thermal energy storage (**Table 2**), is calculated separately for each nodal point for every new time step. The latent heat of melting and evaporation are also taken into consideration for temperature calculation. Finally, different relative speeds are considered by moving the heat source along the workpiece surface.

4.2 Simulation results

Different materials have been first tested and compared, aiming to validate the proposed model. **Figs. 7** and **8** show single craters simulated for bronze (CuSn7Zn4Pb7-C) and steel (AISI1010) respectively. The melting temperature T_{melt}, mass density ρ, specific heat c_p and the thermal conductivity k are shown in the figures. The amount of nodal points in the melting pool, which are represented by a red dark color in both figures, were calculated and relatively compared to experimental results. For a chosen set of erosion parameters, the experimentally measured material removal rate was 11.6 mm^3/min and 5.1 mm^3/min, respectively for bronze and steel. The simulated amounts of nodal points within the melting pool were $2.55x10^5$ and $1.26x10^5$ respectively for bronze and steel. These results represent a experimentally measured relative material removal rate of 44% (dividing steel by bronze) and a simulated relative material removal rate of 49%, showing a good correlation between experimental and simulation results.

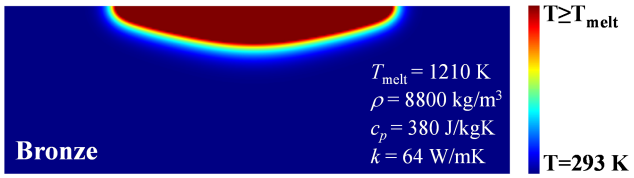

Fig. 7 – Simulation of a single discharge in bronze (I_{peak}=73 A, t_e=1.20 µs).

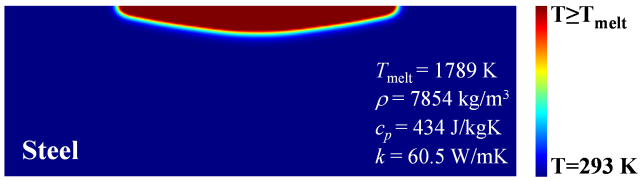

Fig. 8 – Simulation of a single discharge steel (I_{peak}=73 A, t_e=1.20 µs).

Moreover, measurements of material removal rate were carried out for different discharge currents, for steel (AISI1010), and compared to simulation results. **Fig. 9** shows the results obtained for six different discharge currents (*I1- I6*), where a specific discharge current (*I1*) was taken as reference. The peak currents used were as follows: *I1*=73 A; *I2*=84 A; *I3*=124 A; *I4*=157 A; *I5*=223 A; *I6*=276 A. Similar to the above presented results, one can see that there is a good correlation between experimental and simulation results.

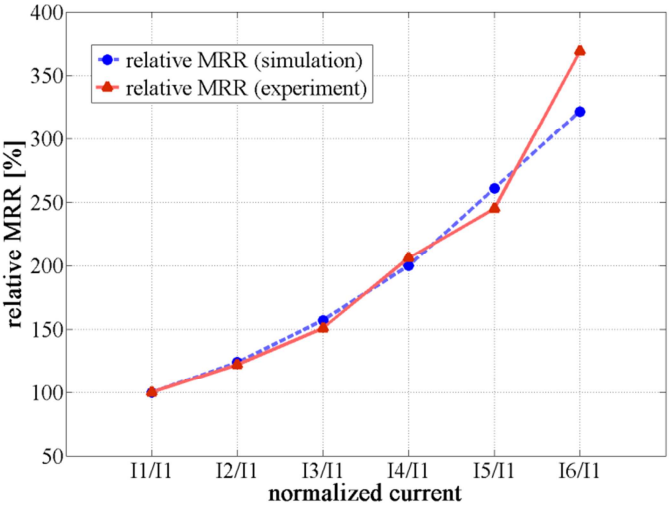

Fig. 9 – Relative material removal rate for different discharge currents (Workpiece: AISI1010).

After validating the model, the next step was to simulate the influence of the relative speed on single discharges. **Fig. 10** shows different simulated cross sections of eroded craters (in speed direction), using brass (CuZn39Pb3) as workpiece material, and relative speeds ranging from v_r =0 to 80 m/s. The heat source slides over the workpiece surface, in this case along the x-axis, creating an elongated crater in this direction.

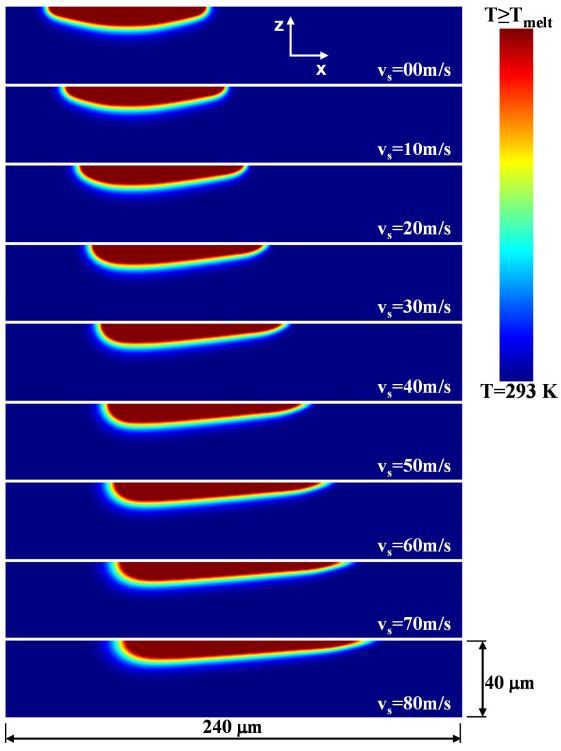

Fig. 10 – Influence of relative speed on single discharges (Brass, I_{peak}=73 A, t_e=1.20 µs).

The influence of the relative speed on the amount of nodal points within the melting pool was calculated and is presented in **Fig. 11**.

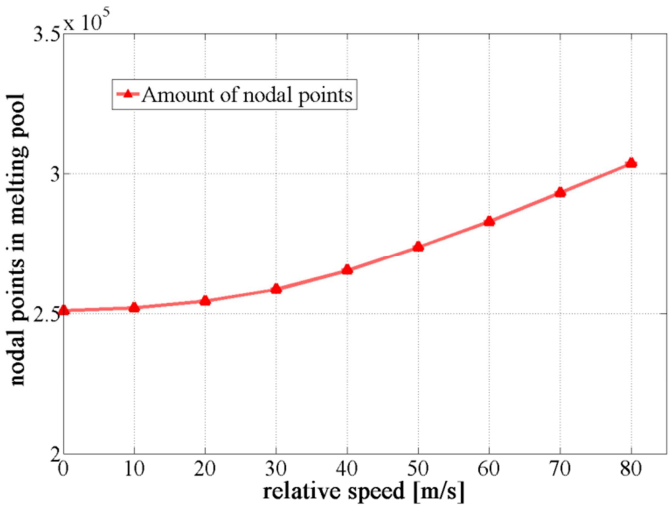

Fig. 11 – Amount of nodal points in the melting pool by increasing relative speed.

One can see that the amount of nodal points that reached temperatures higher than the melting temperature of brass (T_{melt} = 1180 K) increases as relative speed increases. These results are consistent with what was presented in **Fig. 6,** where the measured crater volume was found to increase by increasing the relative speed. Furthermore, the average nodal temperature, taking in consideration all nodes that have reached temperatures higher than the melting temperature, was calculated for different relative speeds and is shown in **Fig. 12**.

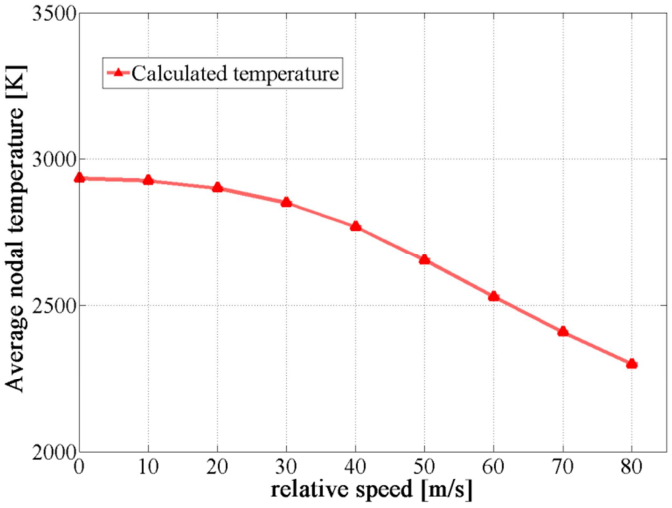

Fig. 12 – Influence of relative speed on the average nodal temperature for nodes which have reached temperatures higher than the melting temperature (Brass: T_{melt} = 1180 K).

It is clear to see that the average nodal temperature decreases by increasing the relative speed, indicating that higher melting efficiencies are obtained for higher relative speeds, where the discharge energy is more efficiently used for warming up and melting more material rather than for further overheating the melting pool.

6. Conclusions

In this study the influence of the relative speed between tool and workpiece electrodes was evaluated for the wire electrical discharge machining process. Single discharge tests were carried out for relative speeds v_r up to 80 m/s. The shape and volume of the eroded craters, measured on the workpiece/anode, were analyzed. According to the measured crater shapes it is possible to see that the plasma channel easily slides over the workpiece/anode. The crater extends along the direction of relative speed and has a slightly reduction of its diameter perpendicular to it. The slip of the center point of the plasma channel was measured and found to match to the theoretical slip, which is calculated based on the applied relative speed and discharge duration. The expansion speed of the crater radius can also be measured based on the shape of eroded craters. It was found that, for a specific set of erosion parameters (I_{peak}=73 A, t_e=1.20 µs), the crater radius expands at a speed of approximately 41 m/s (perpendicular to the slip direction). The eroded volume per crater was found to increase with increasing relative speeds, having a positive impact on the material removal rate. To help explaining the influence of the relative speed on WEDM, an erosion model was proposed based on heat conduction. The finite-difference method was used for solving the partial differential equation that describes heat conduction. The model was validated by comparing simulation and experimental results, where a good consistency was found. Based on simulation results, one can see that the amount of nodal points in the melting pool increases as relative speed increases, being in accordance to the experimental results. The calculated average temperature within the melting pool decreases by increasing the relative speed, indicating that a higher melting efficiency can be reached for higher relative speeds. In this case discharge energy is more efficiently used for warming up and melting material, rather than for extra overheating the melting pool.

For further improvements of the erosion model, we suggest that the following aspects should be taken into consideration:

- Energy distribution: the amount of energy which goes to the anode is unknown and there is no consensus within the academy. It depends, among others, on the type of discharge, the duration time, type of dielectric, pair of materials and discharge pulse intensity. The absolute amount of removed material per discharge is highly influenced by the amount of energy flux which enters the workpiece. By measuring the temperature distribution on the electrodes and

dielectric, one can estimate the energy distribution during the process. This approach was already used by Xia et al. (1996) and has to be further investigated for discharges similar to those used in this work (WEDM);

- Recast layer: The amount of molten material which resolidifies after the discharge is unknown. Using the whole amount of molten material (nodal points in the melting pool) as removed material is not the right approach, since a considerable amount of material stays adhered to the electrode at the end of the discharge. The recast layer can be measured for single craters and is suggested for further improvements of the model. A correlation between recast layer and input energy should be investigated;

Acknowledgments

The authors would like to thank Studer AG, GF AgieCharmilles, Diametal AG, Blaser Swisslube AG, CeramTec AG, and CTI of Switzerland for their support.

References

Haddad, M.J., Tehrani, A.F., 2008. Investigation of cylindrical wire electrical discharge turning (CWEDT) of AISI D3 tool steel based on statistical analysis. Journal of Materials Processing Technology 198, 77-85.

Incropera, F., DeWitt, D., Bergman, T., Lavine, A., 2006. Fundamentals of Heat and Mass Transfer, sixth ed. John Wiley & Sons, Hoboken NJ, pp. 70-73.

Kunieda, M., Kameyama, A., 2010. Study on decreasing tool wear in EDM due to arc spots sliding on electrodes. Precision Engineering 34, 546-553.

Masuzawa, T., Fujino, M., Kobayashi, K., Suzuki, T., Kinoshita, N., 1985. Wire Electro-Discharge Grinding for Micro-Machining. CIRP Annals - Manufacturing Technology 34, 431-434.

Matoorian, P., Sulaiman, S., Ahmad, M.M.H.M., 2008. An experimental study for optimization of electrical discharge turning (EDT) process. Journal of Materials Processing Technology 204, 350-356.

Mohammadi, A., Tehrani, A.F., Emanian, E., Karimi, D., 2008. Statistical analysis of wire electrical discharge turning on material removal rate. Journal of Materials Processing Technology 205, 283-289.

Uhlmann, E., Piltz, S., Jerzembeck, S., 2005. Micro-machining of cylindrical parts by electrical discharge grinding. Journal of Materials Processing Technology 160, 15-23.

Van Elsen, M., Baelmans, M., Mercelis, P., Kruth, J.P., 2007. Solutions for modelling moving heat sources in a semi-infinite medium and applications to laser material processing. International Journal of Heat and Mass Transfer 50, 4872-4882.

Wang, Y., Zhou, X.J., Hu, D.J., 2006. An experimental investigation of dry-electrical discharge assisted truing and dressing of metal bonded diamond wheel. International Journal of Machine Tools & Manufacture 46, 333-342.

Weingartner, E., Jaumann, S., Kuster, F., Boccadoro, M., 2010a. Special wire guide for on-machine wire electrical discharge dressing of metal bonded grinding wheels. CIRP Annals - Manufacturing Technology 59, 227-230.

Weingartner, E., Jaumann, S., Kuster, F., Wegener, K., 2010b. On-machine wire electrical discharge dressing (WEDD) of metal-bonded grinding wheels. Int. J. Adv. Manuf. Technol. 49, 1001-1007.

Xia, H., Kunieda, M., Nishiwaki, N., 1996. Removal Amount Difference between Anode and Cathode in EDM Process. International Journal of Electrical Machining 1, 45-52.

List of figure legends

Fig. 1. Schematic representation of experimental setup for performing WEDM single discharge tests.

Fig. 2 – Influence of relative speed on the shape of eroded craters: a) I_{peak} = 58 A, t_e = 1.15 µs; b) I_{peak} = 73 A, t_e = 1.20 µs.

Fig. 3. Crater diameters for different relative speeds (I_{peak} = 58 A, t_e = 1.15 µs).

Fig. 4 – Slip of plasma arc during single discharges. a): I_{peak}=58 A, t_e=1.15 µs; b) I_{peak}=73 A, t_e=1.20 µs.

Fig. 5 – Method for quantifying the expansion speed of the crater radius.

Fig. 6 – Influence of relative speed on eroded volume of single craters (I_{peak}=73 A, t_e=1.20 µs).

Fig. 7 – Simulation of a single discharge in bronze (I_{peak}=73 A, t_e=1.20 µs).

Fig. 8 – Simulation of a single discharge steel (I_{peak}=73 A, t_e=1.20 µs).

Fig. 9 – Relative material removal rate for different discharge currents (Workpiece: AISI1010).

Fig. 10 – Influence of relative speed on single discharges (Brass, I_{peak}=73 A, t_e=1.20 µs).

Fig. 11 – Amount of nodal points in the melting pool by increasing relative speed.

Fig. 12 – Influence of relative speed on the average nodal temperature for nodes which have reached temperatures higher than the melting temperature (Brass: T_{melt} = 1180 K).

List of table legends

Table 1. Set of parameters used on single discharge experiments.

Table 2. Mathematical description of the thermo-physical erosion model (Transient, three dimensional finite-difference equations). Δt is the time interval, Δx the distance between two consecutive nodal points, ρ represents the mass density (kg/m^3), c_p is the specific heat at constant pressure (J/kg·K) and q'' represents the heat flux (W/m^2).